Toxicology Reports 2 (2015) 574–579

Contents lists available at ScienceDirect

Toxicology Reports

journal homepage: www.elsevier.com/locate/toxrep

Short-term changes in intracellular ROS localisation after the silver nanoparticles exposure depending on particle size

Akira Onodera[a,*], Fumiko Nishiumi[b], Kisa Kakiguchi[c], Atsushi Tanaka[a], Nami Tanabe[a], Aki Honma[a], Katsutoshi Yayama[a], Yasuo Yoshioka[d], Kumiko Nakahira[b], Shigenobu Yonemura[c], Itaru Yanagihara[b], Yasuo Tsutsumi[d], Yuichi Kawai[a]

[a] Department of Pharmaceutical Sciences, Kobegakuin University, 1-1-3 Minatojima, Chuo-ku, Kobe 650-8586, Japan
[b] Department of Developmental Medicine, Osaka Medical Centre and Research Institute for Maternal and Child Health, 840 Murodo-cho, Izumi, Osaka 594-1101, Japan
[c] Electron Microscope Laboratory, RIKEN Centre for Developmental Biology, 2-2-3 Minatojima Minami-Cho, Kobe 650-0047, Japan
[d] Department of Toxicology, Graduate School of Pharmaceutical Sciences, Osaka University, 1–6 Yamada-oka, Suita, Osaka 565-0871, Japan

ARTICLE INFO

Article history:
Received 17 September 2014
Received in revised form 11 March 2015
Accepted 11 March 2015
Available online 23 March 2015

Keywords:
Nanomaterial
Oxidative stress
Nanotoxicology

ABSTRACT

Silver nanoparticles (AgNPs) induce the production of reactive oxygen species (ROS) and apoptosis. These effects are enhanced by smaller particles. Using live-cell imaging, we show that AgNPs induced ROS production rapidly in a size-dependent manner after exposure of cells to 70-nm and 1-nm AgNPs (AgNPs-70, AgNPs-1), but not $AgNO_3$. Exposure of cells to 5 μg/mL each of AgNPs-70, AgNPs-1 or $AgNO_3$ for 1 h decreased the cell viability by approximately 40%, 100% and 20%, respectively. ROS were rapidly induced after 5 and 60 min by AgNPs-1 and AgNPs-70, respectively, whereas $AgNO_3$ had no detectable effect. ROS production detected using the reporter dichlorodihydrofluorescein was observed in whole cells and mitochondria 5 and 60 min after exposure to AgNPs-1. The present study is the first, to our knowledge, to report the temporal expression and intracellular localisation of ROS induced by AgNPs.

1. Introduction

The development of nanomaterials as innovative catalysts in cosmetics and pharmaceuticals has progressed dramatically [1,2]. Although there are no reports of human health hazards, animal experiments show that amorphous nanosilica causes complications in pregnancy, and carbon nanotubes induce damage to the testis and cause mesothelioma [3–5]. Moreover, silver nanoparticles (AgNPs) and their coating agents are marketed as powerful antibacterial agents with antineoplastic activity; however, there are safety concerns [6–10].

AgNPs act as antineoplastic drugs by inducing apoptosis. For example, Dalton's lymphoma is a spontaneous and highly invasive T-cell lymphoma that develops as an ascitic tumour in mice and serves as a model for studying tumorigenesis [6]. AgNPs induce apoptosis and reduce the volume of Dalton's lymphoma by activating caspase 3 [6].

Abbreviations: AgNPs, silver nanoparticles; $AgNO_3$, silver nitrate; DCFH-DA, dichlorodihydrofluorescein diacetate; DLA, Dalton's lymphoma ascites; ROS, reactive oxygen species; TEM, transmission electron microscopy.

* Corresponding author. Tel.: +81 78 974 1551; fax: +81 78 974 4665.
E-mail address: onodera@pharm.kobegakuin.ac.jp (A. Onodera).

http://dx.doi.org/10.1016/j.toxrep.2015.03.004
2214-7500/

Moreover, colloidal AgNPs induce apoptosis of the human MCF7 breast cancer cell line but do not affect the viability of normal peripheral blood mononuclear cells [7].

After intravenous injection, ^{125}I-labelled AgNPs accumulate in the liver and spleen and to a lesser degree in the lungs, bone and blood *in vivo* [8]. Moreover, AgNPs administered orally to rats for 28 days accumulate in the small intestine, stomach, liver, kidney and spleen, and small amounts accumulate in brain and muscle tissues as well [9]. Such effective tissue accumulation of AgNPs warrants further investigation and drug design. However, the extent of inflammation of the blood–brain barrier and induction of the cytokines PGE2, TNF-α and IL-1β in primary rat brain microvessel endothelial cells is inversely proportional to the size of AgNPs [10]. Moreover, binding of AgNPs to GCNF/Fyu kinase in spermatogonial stem cells may inhibit cell proliferation [11]. Therefore, these toxicological issues are important considerations for the effective use of AgNPs.

Induction of ROS by AgNPs is indisputably a primary mechanism of toxicity. Similarly, treatment with radiation and various chemicals directly and indirectly produce ROS, leading to DNA damage and induction of inflammatory cytokines [12]. Analysis of mouse fibroblasts and human hepatocytes reveals that an increase in ROS levels induced by AgNPs is accompanied by a reduction of mitochondrial membrane potential, release of cytochrome C into the cytosol, JNK activation and translocation of Bax to mitochondria [13,14]. The antiapoptotic protein Bcl2 is expressed at high levels by human HCT116 colon cancer cells that are resistant to AgNPs [13]. Further, AgNPs and Ag^+ mediate ROS generation, including superoxide ($O_2^{\bullet -}$), hydroxyl radicals ($^{\bullet}OH$) and hydrogen peroxide (H_2O_2) in cell-free systems [15,16]. Whether the toxicity of AgNPs toxicity is caused by Ag^+, the nanoparticle structure or other factors is unknown.

Therefore, it is important to determine the location and temporal expression of ROS induced by AgNPs. In the present study, we used live-cell imaging with the fluorescent ROS probe dichlorodihydrofluorescein diacetate (DCFH-DA) to investigate the spatiotemporal kinetics of ROS production induced by AgNPs and $AgNO_3$.

2. Materials and methods

2.1. Cell culture

Cryopreserved BALB/3T3 A31-1-1 cells were obtained from the RIKEN Bioresource Centre (Ibaraki, Japan) and were thawed and used for experiments after varying periods. Cells were treated with trypsin and then subcultured three times per week to maintain subconfluent growth. Cells were cultured in Eagle's minimum essential medium (Wako Chemicals) containing 5% foetal calf serum at 37 °C in a humidified atmosphere containing 5% CO_2.

2.2. Silver nanoparticles and other reagents

We purchased 70-nm AgNPs designated AgNPs-70 (AGS-WP001) and 1-nm AgNPs designated AgNPs-1 (AGS-WP001C) from Polytech & Net, GmbH. Particle size distributions were evaluated using dynamic light scattering (DLS) (Fig. 1), which was performed in Hank's Balanced Salt Solution (HBSS) at 25 °C using an ELSZ-2 particle-size analyser (Otsuka Electronics). AgNPs were suspended in HBSS, sonicated for 5 min, and vortexed for 5 min before use. Silver nitrate ($AgNO_3$) and DCFH-DA were purchased from Sigma–Aldrich, Japan. Mito Tracker was purchased from Invitrogen.

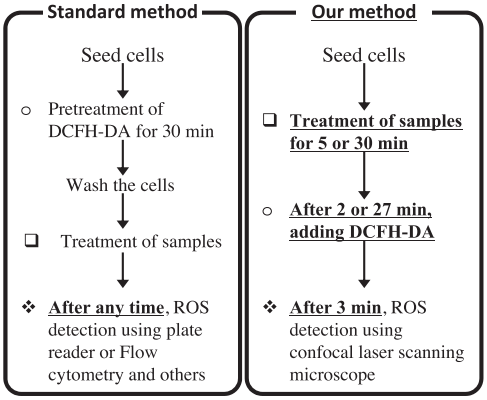

Fig. 1. Physicochemical characterisation of silver nanoparticle suspensions.

2.3. Cell cytotoxicity assay

The cytotoxicities of AgNPs and $AgNO_3$ were determined using a colony formation assay. BALB/3T3 A31-1-1 cells were seeded at 100 cells per dish (60-mm diameter) in culture medium. After incubation for 24 h, the cells were treated for 60 min with AgNPs-70, AgNPs-1 or $AgNO_3$ at 1, 5 and 10 μg/mL [17,18]. After 2 weeks, the cells were fixed with methanol, stained with Giemsa solution, and the colonies were counted. Colonies comprising more than 50 cells were scored [19].

2.4. Live-cell ROS imaging

Intracellular ROS levels were assayed using DCFH-DA, which is cleaved by nonspecific esterases to generate DCFH, and quantitatively oxidised by ROS to generate fluorescent DCF. In the present study, the location of intracellular ROS was imaged using the protocol as follows (Fig. 1): Cells were seeded at 1×10^3 cells per multiwell glass bottom dish (Matsunami). After incubation at 37 °C for 24 h, cells were treated with 1 μM Mito Tracker (Invitrogen) for 30 min, washed twice with culture medium and then exposed to AgNPs or $AgNO_3$ for 5 or 30 min. After 2 or 27 min, the cells were incubated with 10 μM DCFH-DA for 3 min. Live-cell imaging was performed using a FluoView FV1000 confocal laser scanning microscope (Olympus), and the images were analysed using fv10-asw 2.0 viewer software (Olympus). Cells were imaged using an inverted microscope (IX81, Olympus) equipped with a 40× or 100× objective lens. DCF or MitoTracker were excited at 473 nm or 559 nm, respectively, and their emission was detected at 520 nm or 598 nm, respectively. The assay was performed in triplicate in three independent experiments.

2.5. Transmission electron microscopy (TEM)

The intracellular distribution of AgNPs-1 was determined using TEM. Cells were seeded at 1×10^3 cells per microscope cover glass (Fisher scientific). After incubation at 37 °C for 24 h, cells were treated with 5 μg/mL AgNPs-1 for 5 or 60 min, fixed in 0.1 M cacodylate buffer (pH 7.4) containing 2.5% glutaraldehyde and 2.0% paraformaldehyde, fixed again using 1% OsO_4 in 0.1 M cacodylate buffer (pH 7.4), stained en bloc with 0.5% aqueous uranyl acetate and dehydrated using a graded series of ethanol concentrations. Samples were embedded in resin (Poly/Bed 812; Polysciences, Inc.), and ultrathin sections were stained with uranyl acetate and lead citrate and observed using an electron microscope (JEM-1010; JEOL).

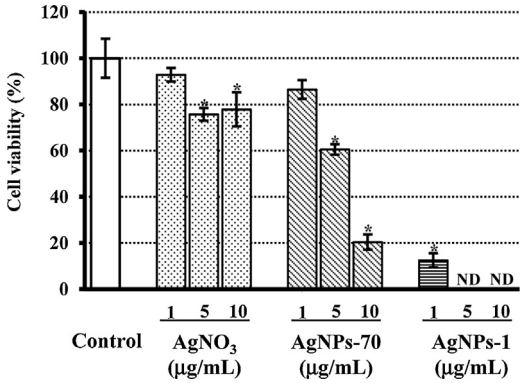

Fig. 2. Cytotoxicity of AgNPs and $AgNO_3$. The cell viability of BALB/3T3 cells was determined using a colony formation assay described in Section 2. ND, Not detected. $^*P < 0.05$ *vs.* control (ANOVA and Tukey's HSD tests).

3. Results and discussion

The purpose of the present study was to determine the relationship of AgNP particle size to cytotoxicity and the generation of ROS. For this purpose, we used AgNPs-70 and AgNPs-1 as well as $AgNO_3$ as a source of Ag^+. The particle sizes chosen are consistent with evidence that gave rise to the theory that smaller particles are more toxic. DLS measurements using the ELSZ-2 particle-size analyser show that the average particle diameter of AgNPs-70 was 63.5 nm, the surface electric charge was −0.98 mV and the polydispersity index (PDI) was 0.238 (Table 1). The

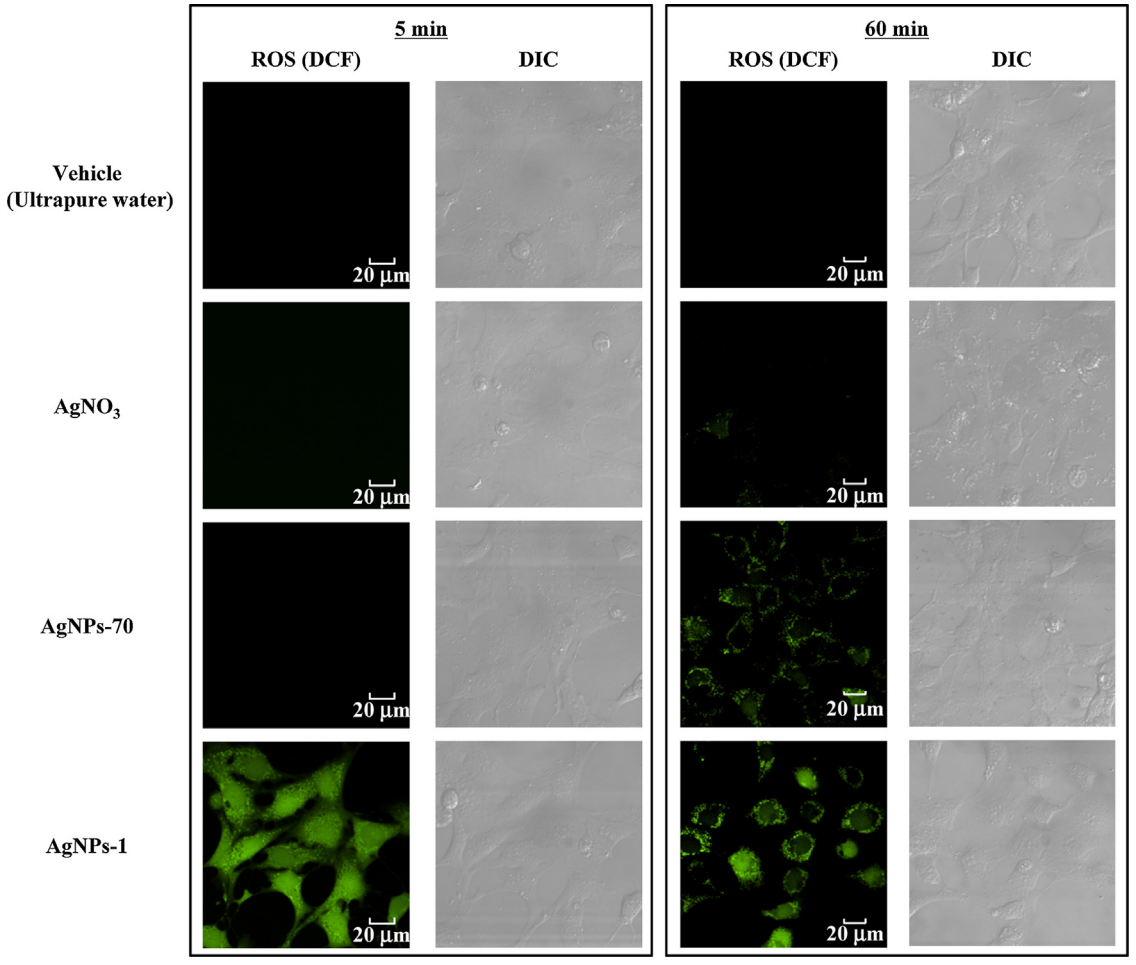

Fig. 3. Location and temporal expression of intracellular ROS induced by AgNPs. Cells were treated with 5 μg/mL $AgNO_3$, AgNPs-70 or AgNPs-1 for 5 or 30 min and stained with MitoTracker after 30 min. ROS imaging was conducted 3 min after the cells were labelled with DCFH-DA.

Table 1
Physicochemical characterisation of silver nanoparticle suspensions.

	Diameter (nm)	Polydispersity index (PDI)	ζ-potential (mV)
70-nm AgNPs	63.5 ± 1.04	0.238 ± 0.007	−10.98 ± 0.51
1-nm AgNPs	1.2 ± 0.54	N.D.	−13.45 ± 1.23

All data are expressed as the mean ± SD.

average particle diameter of AgNPs-1 was 1.2 nm, the surface electric charge was −13.45 mV and the PDI could not be measured (Table 1).

Next, we evaluated the cytotoxicity of $AgNO_3$ and AgNPs using a colony formation assay. It is assumed that the toxicity of silver nanoparticles is caused by silver ion or nanoparticle form and both [20]. Accordingly, the cell viability was approximately 78% at 10-μg/mL AgNO3, and, approximately 21% and 0% of cell viability were observed at AgNPs-70 and AgNPs-1, respectively, at the same Ag concentration. Thus, after 1-h treatments, toxicity of AgNPs was predominantly mediated by nanoparticles form rather than silver ion.

These results indicate that the smaller silver particles were more cytotoxic and are consistent with the tentative theory that smaller AgNPs are more cytotoxic [20].

We next asked if this common theory applied to the induction of ROS by AgNPs. For this purpose, we treated cells with DCFH-DA for 3 min before conducting intracellular imaging to avoid difficulties of the standard 30 min treatment. We determined that DCFH reacted with ROS and accumulated as DCF in the cytoplasm at approximately 30 min, which would interfere with the detection of ROS in organelles. DCF was detected in the cytoplasm and mitochondria after exposure to AgNPs-1 for 5 min (Fig. 3) but not to AgNPs-70 or $AgNO_3$ (Fig. 3). After 60 min exposure to AgNPs-70 and AgNPs-1, but not to $AgNO_3$, increased the levels of DCF were mainly observed in mitochondria (Figs. 3 and 4).

When cells were exposed to amorphous nanosilica particles, which produce ROS through plasma membrane NADPH oxidase under the experimental conditions employed here (see Section 2.4), DCF was observed throughout the entire cell, and the fluorescence intensity increased with time (Supplementary Fig. 1) [21]. Moreover, the fluorescence intensity profiles of MitoTracker and DCF were almost completely consistent. In particular, DCF fluorescence was detected between the peaks of the mitochondrial membrane, which were swollen by AgNPs-1 (Fig. 4). These results strongly suggest that AgNPs-70 and AgNPs-1 induced mitochondrial ROS production in a size-dependent manner (Fig. 3). Moreover, the increasing tendency of the fluorescence intensity was apparent in the presence of AgNPs-1 than in the presence of AgNPs-70,

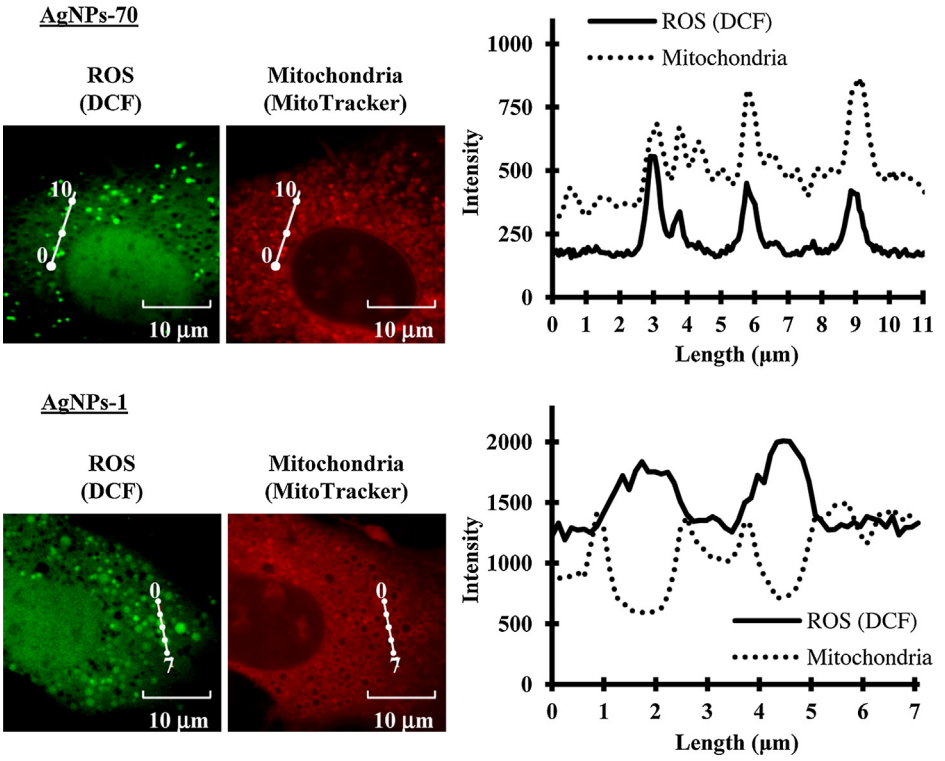

Fig. 4. Fluorescence intensity profile graphs of AgNP-induced mitochondrial ROS. The graphs show the intensity of DCF and MitoTracker fluorescence. Upper and lower images and line charts show cells 60 min after treatment with AgNPs-1 and AgNPs-70, respectively.

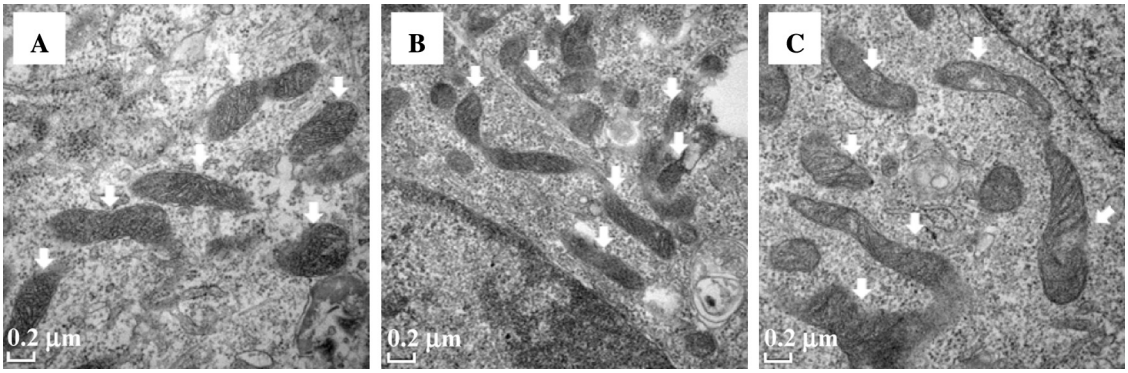

Fig. 5. TEM images of ultrathin cell sections. The image shows mitochondria (white arrow) in untreated cells (A) and cells treated with 5 μg/mL AgNPs-1 for 5 min (B) and 60 min (C).

indicating increased mitochondrial ROS production in the presence of smaller AgNPs (Figs. 3 and 4). It was thought that $AgNO_3$ could be used as a model for Ag ion because it had less cytotoxicity due to weak ROS production by mitochondria (Figs. 2 and 3).

To determine whether AgNPs directly induced mitochondrial ROS, we used TEM to examine the localisation of AgNPs-1 in mitochondria. AgNPs-1 were not detected in mitochondria after 5 and 60 min of exposure (Fig. 5); however, it was difficult to visualise 1-nm particles. However, because AgNPs-1 induced ROS production by mitochondria, this may be an indirect effect associated with redox signalling by intracellular ROS. The contribution of intracellular ROS to redox signalling in intracellular organelles indicates roles in addition to the oxidation of DNA and lipids. Increased mitochondrial ROS levels affect redox potentials and the thiol-disulphide redox states of ATP/ADP translocators, causing the opening of permeability transition pores and the induction of apoptosis [22]. Moreover, increased levels of intranuclear ROS enhance hypoxia-sensitive gene expression by oxidising DNA encoding hypoxia response elements [23]. Specifically, the plasma membrane NADPH oxidase family member Nox3, which is induced by ROS, promotes TNFα production and Fas-mediated apoptosis through c-Jun N-terminal kinase signalling [24,25]. ROS induce the expression of Nox4, which resides in the endoplasmic reticulum, and mediates the oxidation of PTP1B and EGF signalling [26]. Therefore, the production of ROS by specific organelles triggers apoptosis in a manner similar to that induced by the cytotoxic effects of AgNPs.

4. Conclusions

The present report provides the evidence acquired using live-cell imaging that AgNPs induced the production of ROS by mitochondria after only 5 and 60 min. Further, the smaller AgNPs particles induced higher levels of mitochondrial ROS. Increased mitochondrial ROS induce cell death by promoting intrinsic apoptotic pathways [27,28], and we conclude that AgNPs induce apoptosis by this mechanism. It is possible that increased oxidation of DNA is caused by cellular internalisation of AgNPs. However, the mechanisms of nanoparticle internalisation are unclear and may be associated with destabilisation of cell membranes [29,30]. AgNPs are powerful inducers of cell death compared with other nanoparticles. We hypothesise that AgNPs induce cytotoxicity after they are internalised.

Transparency document

The Transparency document associated with this article can be found in the online version.

Conflict of interest statement

There are no competing interests.

Acknowledgements

This study was supported in part by Health Labour Sciences Research Grants from the Ministry of Health, Labour and Welfare of Japan (MHLW), the Japan Food Chemical Research Foundation and Kobegakuin University Grant C.

Appendix A. Supplementary data

Supplementary data associated with this article can be found, in the online version, at doi:10.1016/j.toxrep.2015.03.004.

References

[1] S. Singh, A. Sharma, G.P. Robertson, Realizing the clinical potential of cancer nanotechnology by minimizing toxicologic and targeted delivery concerns, Cancer Res. 72 (2012) 5663–5668.
[2] S. Raj, S. Jose, U.S. Sumod, M. Sabitha, Nanotechnology in cosmetics: opportunities and challenges, J. Pharm. Bioallied Sci. 4 (2012) 186–193.
[3] K. Yamashita, Y. Yoshioka, K. Higashisaka, K. Mimura, Y. Morishita, M. Nozaki, T. Yoshida, T. Ogura, H. Nabeshi, K. Nagano, Y. Abe, H. Kamada, Y. Monobe, T. Imazawa, H. Aoshima, K. Shishido, Y. Kawai, T. Mayumi, S. Tsunoda, N. Itoh, T. Yoshikawa, I. Yanagihara, S. Saito, Y. Tsutsumi, Silica and titanium dioxide nanoparticles cause pregnancy complications in mice, Nat. Nanotechnol. 6 (2011) 321–328.
[4] Y. Bai, Y. Zhang, J. Zhang, Q. Mu, W. Zhang, E.R. Butch, S.E. Snyder, B. Yan, Repeated administrations of carbon nanotubes in male mice cause reversible testis damage without affecting fertility, Nat. Nanotechnol. 5 (2010) 683–689.
[5] H. Nagai, Y. Okazaki, S.H. Chew, N. Misawa, Y. Yamashita, S. Akatsuka, T. Ishihara, K. Yamashita, Y. Yoshikawa, H. Yasui, L. Jiang, H. Ohara, T. Takahashi, G. Ichihara, K. Kostarelos, Y. Miyata, H. Shinohara, S. Toyokuni, Diameter and rigidity of multiwalled carbon nanotubes are

critical factors in mesothelial injury and carcinogenesis, Proc. Natl. Acad. Sci. U. S. A. 108 (2011) 1330–1338.
[6] M.I. Sriram, S.B. Kanth, K. Kalishwaralal, S. Gurunathan, Antitumor activity of silver nanoparticles in Dalton's lymphoma ascites tumor model, Int. J. Nanomed. 5 (2010) 753–762.
[7] M.A. Franco-Molina, E. Mendoza-Gamboa, C.A. Sierra-Rivera, R.A. Gómez-Flores, P. Zapata-Benavides, P. Castillo-Tello, J.M. Alcocer-González, D.F. Miranda-Hernández, R.S. Tamez-Guerra, C. Rodríguez-Padilla, Antitumor activity of colloidal silver on MCF-7 human breast cancer cells, J. Exp. Clin. Cancer Res. 29 (2010) 148.
[8] A. Chrastina, J.E. Schnitzer, Iodine-125 radiolabeling of silver nanoparticles for in vivo SPECT imaging, Int. J. Nanomed. 5 (2010) 653–659.
[9] K. Loeschner, N. Hadrup, K. Qvortrup, A. Larsen, X. Gao, U. Vogel, A. Mortensen, H.R. Lam, E.H. Larsen, Distribution of silver in rats following 28 days of repeated oral exposure to silver nanoparticles or silver acetate, Part Fibre Toxicol. 1 (2011) 8–18.
[10] W.J. Trickler, S.M. Lantz, R.C. Murdock, A.M. Schrand, B.L. Robinson, G.D. Newport, J.J. Schlager, S.J. Oldenburg, M.G. Paule, W. Slikker Jr., S.M. Hussain, S.F. Ali, Silver nanoparticle induced blood-brain barrier inflammation and increased permeability in primary rat brain microvessel endothelial cells, Toxicol. Sci. 118 (2010) 160–170.
[11] L.K. Braydich-Stolle, B. Lucas, A. Schrand, R.C. Murdock, T. Lee, J.J. Schlager, S.M. Hussain, M.C. Hofmann, Silver nanoparticles disrupt GDNF/Fyn kinase signaling in spermatogonial stem cells, Toxicol. Sci. 116 (2010) 577–589.
[12] J.E. Klaunig, Z. Wang, X. Pu, S. Zhou, Oxidative stress and oxidative damage in chemical carcinogenesis, Toxicol. Appl. Pharmacol. 254 (2011) 86–99.
[13] Y.H. Hsin, C.F. Chen, S. Huang, T.S. Shih, P.S. Lai, P.J. Chueh, The apoptotic effect of nanosilver is mediated by a ROS- and JNK-dependent mechanism involving the mitochondrial pathway in NIH3T3 cells, Toxicol. Lett. 179 (3) (2008) 130–139.
[14] M.J. Piao, K.A. Kang, I.K. Lee, H.S. Kim, S. Kim, J.Y. Choi, J. Choi, J.W. Hyun, Silver nanoparticles induce oxidative cell damage in human liver cells through inhibition of reduced glutathione and induction of mitochondria-involved apoptosis, Toxicol. Lett. 201 (1) (2011), 92–10.
[15] D. He, A.M. Jones, S. Garg, A.N. Pham, T.W. David, Silver nanoparticle–reactive oxygen species interactions: application of a charging–discharging model, J. Phys. Chem. C 115 (2011) 5461–5468.
[16] D. He, S. Garg, T.D. Waite, H_2O_2-mediated oxidation of zero-valent silver and resultant interactions among silver nanoparticles, silver ions, and reactive oxygen species, Langmuir 28 (2012) 10266–10275.
[17] C. Yasutake, Y. Kuratomi, M. Ono, S. Masumi, M. Kuwano, Effect of 5-azacytidine on malignant transformation of a mutant derived from the mouse BALB/c 3T3 cell line resistant to transformation by chemical carcinogens, Cancer Res. 47 (1987) 4894–4899.
[18] D.J. Fitzgerald, C. Piccoli, H. Yamasaki, Detection of non-genotoxic carcinogens in the BALB/c 3T3 cell transformation/mutation assay system, Mutagenesis 4 (1989) 286–291.
[19] T. Tsuchiya, M. Umeda, Improvement in the efficiency of the in vitro transformation assay method using BALB/3T3 A31-1-1 cells, Carcinogenesis 16 (1995) 1887–1894.
[20] N. Lubick, Nanosilver toxicity: ions, nanoparticles – or both? Environ. Sci. Technol. 42 (23) (2008) 8617.
[21] H. Nabeshi, T. Yoshikawa, K. Matsuyama, Y. Nakazato, S. Tochigi, S. Kondoh, T. Hirai, T. Akase, K. Nagano, Y. Abe, Y. Yoshioka, H. Kamada, N. Itoh, S. Tsunoda, Y. Tsutsumi, Amorphous nanosilica induce endocytosis-dependent ROS generation and DNA damage in human keratinocytes, Part Fibre Toxicol. 8 (2011) 1.
[22] T. Xia, C. Jiang, L. Li, C. Wu, Q. Chen, S.S. Liu, A study on permeability transition pore opening and cytochrome c release from mitochondria, induced by caspase-3 in vitro, FEBS Lett. 510 (2002) 62–66.
[23] M.P. Murphy, Modulating mitochondrial intracellular location as a redox signal, Sci. Signal. 5 (2012) pe39.
[24] Y. Suzuki, Y. Ono, Y. Hirabayashi, Rapid and specific reactive oxygen species generation via NADPH oxidase activation during Fas-mediated apoptosis, FEBS Lett. 425 (1998) 209–212.
[25] L. Li, Q. He, X. Huang, Y. Man, Y. Zhou, S. Wang, J. Wang, J. Li, NOX3-derived reactive oxygen species promote TNF-alpha-induced reductions in hepatocyte glycogen levels via a JNK pathway, FEBS Lett. 584 (2010) 995–1000.
[26] K. Chen, M.T. Kirber, H. Xiao, Y. Yang, J.F. Keaney Jr., Regulation of ROS signal transduction by NADPH oxidase 4 localization, J. Cell Biol. 181 (2008) 1129–1139.
[27] M.L. Circu, T.Y. Aw, Reactive oxygen species cellular redox systems, and apoptosis, Free Radic. Biol. Med. 48 (2010) 749–762.
[28] B. Herrera, A.M. Alvarez, A. Sánchez, M. Fernández, C. Roncero, M. Benito, I. Fabregat, Reactive oxygen species (ROS) mediates the mitochondrial-dependent apoptosis induced by transforming growth factor (beta) in foetal hepatocytes, FASEB J. 15 (2001) 741–751.
[29] J. Lechner, N. Malloth, T. Seppi, B. Beer, P. Jennings, W. Pfaller, IFN-alpha induces barrier destabilization and apoptosis in renal proximal tubular epithelium, Am. J. Physiol. Cell Physiol. 294 (2008) 153–160.
[30] V. Bandmann, J.D. Müller, T. Köhler, U. Homann, Uptake of fluorescent nano beads into BY2-cells involves clathrin-dependent and clathrin-independent endocytosis, FEBS Lett. 586 (2012) 3626–3632.